PCCP

PAPER

View Article Online
View Journal | View Issue

Cite this: *Phys. Chem. Chem. Phys.*, 2017, **19**, 27212

Intriguing transport dynamics of ethylammonium nitrate–acetonitrile binary mixtures arising from nano-inhomogeneity†

Alessandro Mariani, ‡*[a] Matteo Bonomo,[a] Boning Wu,[b] Barbara Centrella,[a] Danilo Dini,[a] Edward W. Castner Jr.[b] and Lorenzo Gontrani *[a]

Received 8th July 2017,
Accepted 18th September 2017

DOI: 10.1039/c7cp04592a

rsc.li/pccp

Binary mixtures of ethylammonium nitrate and acetonitrile show interesting properties that originate from the structural and dynamical nano-heterogeneity present in ionic liquids. These effects are most pronounced when the ionic liquid is the minority compound. In this study the transport properties of such mixtures are studied, including viscosity, self-diffusion and conductivity. The results strongly support the presence of structural inhomogeneity and show an interesting composition-dependent behaviour in the mixtures.

Introduction

Transport properties of fluid mixtures are central to many biological and industrial applications. Their understanding is crucial to achieve complete characterization of a system. Recently, more attention has been paid to the mixing behaviour of ionic liquids (ILs) with neutral molecular solvents because the unusual physical and chemical properties of these materials may lead to improved alternatives to common organic solvents.[1–4] Transport properties of binary mixtures containing ionic liquids are attracting increasing attention because of the enhanced mobility of the ions when a co-solvent is added to the system.[5–7] Seddon *et al.* observed the general trend that the viscosity of a mixture containing an IL and an organic co-solvent depends solely on the mole fraction of the additive, and not on its nature.[8] They investigated a series of imidazolium-based ILs mixed with a variety of solvents including water, toluene, 1,4-dimethylbenzene, 1,2-dimethoxyethane, ethanenitrile, 2-propenenitrile and trimethylethanenitrile. They showed how viscosity is monotonically decreased upon increasing the organic mole fraction. A systematic study as a function of temperature and short 1-alcohol content in other imidazolium based ILs was proposed by Domànska *et al.*[9,10] They observed how composition has a much stronger effect than temperature on viscosity. It must be noted that water impurities arising from moisture in the atmosphere could dramatically affect all the transport properties of ionic liquids,[8] for this reason the experiments should be carried out in a controlled atmosphere. EAN is one of the first ever reported room temperature ILs,[11] discovered by Walden in 1914. It has been extensively studied both as a neat compound and as a mixture with other ILs or organic compounds.[12–25] Acetonitrile (ACN or CH_3CN) is a common aprotic polar solvent, widely used in organic chemistry and for electrochemical applications. Binary mixtures of EAN and ACN were studied by Perron *et al.* in 1993,[26] by Mancini *et al.* in 2004[27] and by Sonnleitner *et al.* in 2013.[28] Perron *et al.* first reported the conductivity of the EAN–ACN mixtures, stating that this system shows a nearly ideal behaviour, meaning that ACN simply dilutes the IL leaving it almost unaffected except for very high ACN content where ionic dissociation plays an important role. The new results presented here do not coincide with this interpretation. Mancini *et al.* explored the overall hydrogen bonding properties of EAN–ACN mixtures using different solvatochromic indicators, observing a slightly enhanced acceptor character when acetonitrile is added to EAN. They have stated that this behaviour may suggest the formation of supramolecular complexes. Sonnleitner *et al.* performed dielectric spectroscopy experiments on the mixtures, observing a clear transition between low-EAN and high-EAN concentration regimes in the solvation of the cation.[28] Here the transport properties of binary mixtures containing ethylammonium nitrate and acetonitrile are analysed.

Results and discussion

The experimental viscosities of neat EAN and ACN and their mixtures at different temperatures are reported in Fig. 1. In

[a] *Department of Chemistry, La Sapienza University of Rome, P.le A. Moro 5, 00185 Rome, Italy. E-mail: alessandro.mariani@esrf.fr, lorenzo.gontrani@uniroma1.it*
[b] *Department of Chemistry & Chemical Biology, Rutgers The State University of New Jersey, 610 Taylor Road Piscataway, NJ 08854-8066, USA*

† Electronic supplementary information (ESI) available: Zoomed version of Arrhenius fit graphics; fitting parameters for the Redlich–Kister functions used in the paper; measured conductivities as a function of composition and temperature; a comparison with literature data of conductivity at ambient temperature. See DOI: 10.1039/c7cp04592a

‡ Current address: The TRUSAXS beamline ID02, European Synchrotron Radiation Facility, 71 Avenue des Martyrs, 38000 Grenoble, France.

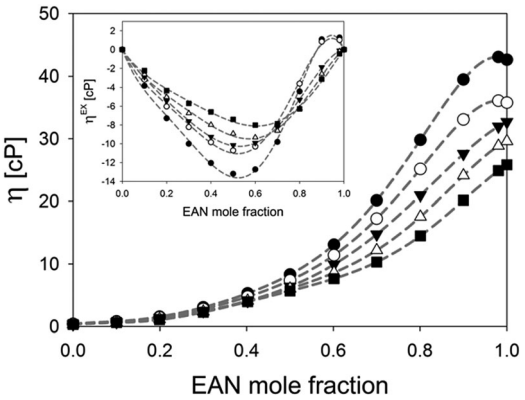

Fig. 1 Viscosity of ethylammonium nitrate–acetonitrile mixtures at different temperatures. (inset) Excess viscosity for the same systems. 288 K (black circles); 293 K (white circles); 298 K (black triangles); 303 K (white triangles); 308 K (black squares). The dashed line in the main frame is just a guide to the eye, while in the inset it represents the fitting of the experimental values.

Table 1 Comparison between viscosity values in this work and in the literature at 298 K for EAN–ACN mixtures

χ_{EAN}	η_{EXP}	η_{LIT}
0	0.350	0.3413[a]
0.1	0.685	0.730[a]–0.676[b]
0.2	1.374	1.43[a]–1.352[b]
0.3	2.451	2.366[b]
0.4	4.067	3.718[b]
0.5	6.370	6.36[a]–5.746[b]
0.6	9.916	9.67[a]–8.788[b]
0.7	14.730	15.1[a]–13.013[b]
0.8	20.967	20.9[a]–18.252[b]
0.9	27.580	—
0.98	31.964	—
1	32.690	38.6[a]–33.8[b]

[a] Data from ref. 28. [b] Data from ref. 26.

Table 1 a comparison between our data and the literature is made and we see good agreement between different sets of data.

When the temperature is equal to or higher than 298 K, the viscosity monotonically decreases as acetonitrile is added to EAN. Interestingly, at lower temperatures addition of a very small quantity of acetonitrile (χ_{EAN} = 0.98) to the IL increases the measured viscosity. Upon further dilution, the trend is the same as for the other temperatures. This unusual behaviour is observed in some water mixtures with alcohols[29,30] and in the toluene–methanol[31] system. The given interpretation is that the formation of micelles has as a consequence the increase of the viscosity, because they can be considered as colloidal particles.[29] Under these particular conditions of composition and temperature, the behaviour of the EAN–acetonitrile mixture diverges from the general law proposed by Seddon *et al.*[8] The inset of Fig. 1 reports the excess viscosity η^{EX} defined as[32,33]

$$\eta^{EX} = \eta_{EXP} - [\chi_{EAN}\cdot\eta_{EAN} + (1 - \chi_{EAN})\cdot\eta_{ACN}] \quad (1)$$

The variables η_{EXP}, η_{EAN} and η_{ACN} are the experimental viscosities of the mixture, neat EAN and of neat acetonitrile, respectively, and χ_{EAN} is the mole fraction of the IL in the mixture. The points obtained from experimental data were fitted using a Redlich–Kister function,[34,35]

$$\xi(\chi_1) = \chi_1(1 - \chi_1)\sum a_n(1 - 2\chi_1)^n \quad (2)$$

where $\xi(\chi_1)$ is any excess property expressed as a function of the mole fraction of component 1 χ_1, and a_n are adjustable parameters. For excess viscosity fitting, the parameters can be found in the ESI† (Table S1). The deviation from the ideal behaviour is more pronounced at lower temperatures, and it appears to be strongly dependent on the temperature passing from a value of −13.62 cP for the minimum at 288 K to −8.11 cP at 308 K, for a change of ∼60%. Moreover, there are two different trends in the curves depending on the temperature. For 298 K, 303 K and 308 K the curves are negative for the whole concentration range, showing a temperature-dependent minimum at χ_{EAN} = 0.53, 0.57 and 0.61 respectively. At 288 K and 293 K, the curve minima occur at χ_{EAN} = 0.52, and a distinct maximum appears in the IL-rich region at χ_{EAN} = 0.95 at both temperatures. This anomaly will be further analysed in an upcoming work. From the viscosity data, the excess Gibbs free energy for the activation of the viscous flow can be obtained by[36,37]

$$\frac{\Delta G^{*EX}}{RT} = \ln\left(\frac{\eta_{EXP}V}{\eta_{ACN}V^{M}_{ACN}}\right) - \chi_{EAN}\ln\left(\frac{\eta_{EAN}V^{M}_{EAN}}{\eta_{ACN}V^{M}_{ACN}}\right) \quad (3)$$

where R is the gas constant, T is the absolute temperature, V^{M} indicates the partial molar volume of a component (derived elsewhere[38]) and V is the total molar volume defined as

$$V = \chi_{EAN}\cdot V^{M}_{EAN} + (1 - \chi_{EAN})\cdot V^{M}_{ACN} \quad (4)$$

The results obtained using eqn (3) are plotted in Fig. 2 along with the fit obtained using a Redlich–Kister function (parameters in the ESI,† Table S2).

The temperature seems to have a stronger than usual effect on the viscosity. The excess Gibbs free energy for the activation of the viscous flow shows positive values in the whole composition range, but two distinct behaviours are observed with

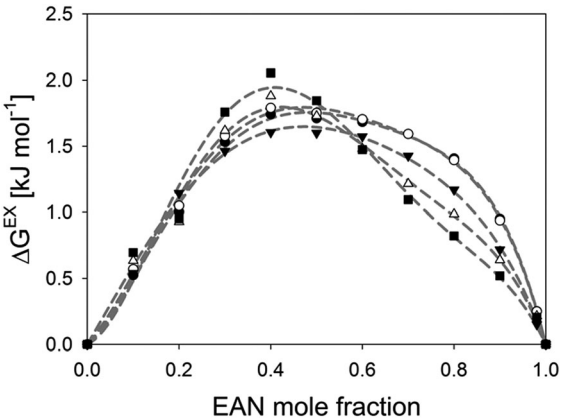

Fig. 2 Excess Gibbs free energy for the activation of viscous flow for ethylammonium nitrate–acetonitrile mixtures at different temperatures. 288 K (black circles); 293 K (white circles); 298 K (black triangles); 303 K (white triangles); 308 K (black squares). The dashed line is the fit of experimental data to eqn (2).

respect temperature. For 303 K and 308 K, a distinct, defined maximum at χ_{EAN} = 0.42 and 0.41, respectively, is observed, whereas at 288 K and 293 K, the curves are much broader and almost identical, with a maximum at χ_{EAN} = 0.47. The 298 K curve lies between the two sets and connects the change from the low temperature to the high temperature regime. As can be seen, a distinct shoulder appears in the IL-rich region when the system is cooled, meaning that under these conditions of temperature and composition, there are some molecular complexes that are harder to set in motion. It is well known that the empirical Vogel–Fulcher–Tammann (VFT) equation provides an excellent fit to the measured viscosities of ILs.[22,39–42] However, since the maximum viscosity measured was about 45 cP, it becomes valid to use the Arrhenius activated power law to describe the temperature dependence of viscosity, since the Arrhenius law is the high temperature limit of the VFT model.[43] Validity of such an approach has been provided elsewhere.[36] The equation used was

$$\ln(\eta_{EXP}) = \ln(\eta_\infty) + \frac{E_a}{R}\cdot\frac{1}{T} \quad (5)$$

where η_∞ is a coefficient of the system that may be interpreted as the hypothetical viscosity at infinite temperature, and E_a is the Arrhenius activation energy of the viscous flow. The resulting fits to the experimental data using eqn (5) are shown in Fig. 3a and the fitting parameters are given in Table 2.

The Arrhenius law appears to provide an excellent description of the mixture behaviour of the system at every composition in the considered temperature range. This is not surprising, because the Arrhenius law is the high temperature limit of the VFT equation as said before, and dilution of EAN by ACN will serve to push the system further towards the high temperature limit. For the EAN-rich systems, a zoomed version of Fig. 3a is found in Fig. S1 in the ESI.†

As a function of the EAN mole fraction χ_{EAN}, the activation enthalpy E_a shows three distinct trends. Up to χ_{EAN} 0.4, the value increases gradually (~20% increase from χ_{EAN} 0.1 to χ_{EAN} 0.4) and it is always similar to the value for neat acetonitrile. Upon further increasing the χ_{EAN}, the activation energy steeply increases up to χ_{EAN} = 0.8. In the most concentrated EAN region, E_a decreases. These trends correspond to the various regions of η^{EX}. The initial slow increase in E_a overlaps with the excess viscosity decrease, the steep increase in the energy overlaps with the rapid raise of η^{EX} and, finally, the decrease in the EAN-rich region corresponds to the decrease in the excess viscosity after the maximum (in the low temperature regime). Interestingly, the maximum position in E_a is the same as for the shoulder in the excess Gibbs activation energy. This odd behaviour may be linked to some structural transition. In neat EAN, the molecules are organized in a well-known sponge-like arrangement,[44] upon addition of acetonitrile, the activation energy increases because of the formation of some supramolecular structures – as mentioned for the increased viscosity of the χ_{EAN} = 0.98 mixture – that require more energy to be set in motion. This effect has a maximum at χ_{EAN} = 0.8. From that point on, the supramolecular structures are progressively dissolved, resulting in the decrease of the activation energy of viscous flow.

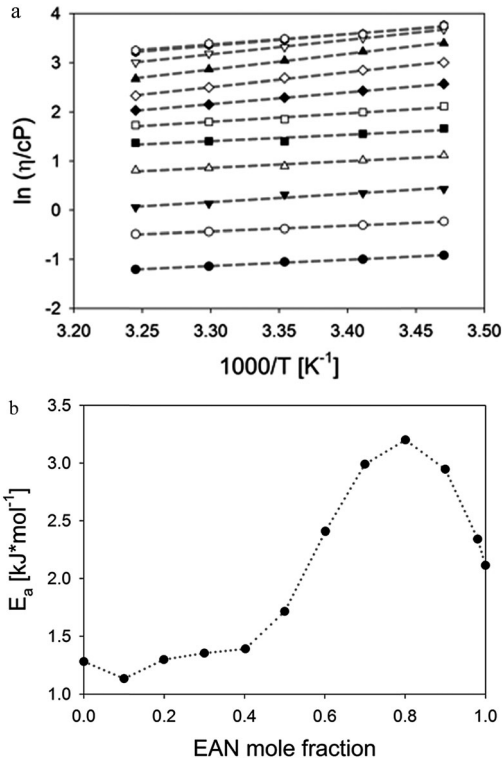

Fig. 3 (a) Arrhenius plot for the ethylammonium nitrate–acetonitrile mixtures at various compositions. χ_{EAN} = 0 (black circles); 0.1 (white circles); 0.2 (black reversed triangles); 0.3 (white triangles); 0.4 (black squares); 0.5 (white squares); 0.6 (black diamonds); 0.7 (white diamonds); 0.8 (black triangles); 0.9 (white reversed triangles); 0.98 (black hexagons); 1 (white hexagons). The dashed lines indicate Arrhenius fits. (b) Arrhenius activation energy of the viscous flow. Here the dotted line is just a visual guide, not a fit.

Table 2 Arrhenius law fits to the temperature dependent viscosity for EAN–ACN mixtures

χ_{EAN}	E_a [kJ mol^{-1}]	η_∞
0	1.28	−5.35
0.1	1.13	−4.16
0.2	1.30	−5.44
0.3	1.35	−3.60
0.4	1.39	−2.92
0.5	1.72	−3.86
0.6	2.41	−5.79
0.7	2.99	−7.36
0.8	3.20	−7.70
0.9	2.95	−6.55
0.98	2.34	−4.38
1	2.11	−3.60

To further understand the transport properties of the system, we measured the self-diffusion coefficients D for the ethylammonium cation and acetonitrile *via* Pulsed-Gradient Spin-Echo (PGSE) NMR experiments.[45–47] Since the EAN cation and ACN signals are quite distinct in the ^{1}H-NMR spectrum, it is straightforward to measure the diffusivities of each species independently, fitting the peak decay using the equation from Wu *et al.*[47]

$$\ln(I_g) = \ln(I_0) - (\gamma\delta g)^2 D\left(\Delta - \frac{\delta}{3}\right) \quad (6)$$

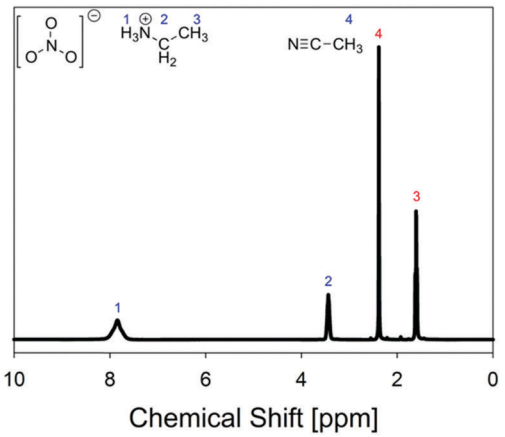

Fig. 4 ^{1}H NMR spectrum of the ethylammonium nitrate–acetonitrile mixture for χ_{EAN} = 0.5. Each peak is assigned to the respective hydrogen atoms in the structure by the numbers. The red numbers indicate the peaks used to calculate the diffusion coefficients.

where g is the applied gradient field strength, I_0 is the signal intensity for $g = 0$, γ is the gyromagnetic constant, Δ is the diffusion delay time, δ is the duration of the gradient pulse, and D is the desired self-diffusion coefficient. As an example, the spectrum of the 1 : 1 mixture are reported in Fig. 4 (the signal of water in the separate external container, was removed for clarity). While it would be possible to measure the anion diffusivity by using a ^{15}N spin-labelled nitrate, we did not attempt the synthesis of this species. All the chemical shifts for each system studied are reported in Table 3.

The NMR signal of samples under a sequence of 15–20 different gradients was measured, and the data were analysed using previously reported methods,[7] so that the diffusion coefficients can be calculated. The gradient is calibrated using a D_2O sample, where the diffusivity of HDO in D_2O is calibrated to 1.9×10^{-5} cm^2 s^{-1} at 298 K. The diffusion coefficients of the cation and acetonitrile are measured using ^{1}H resonances at ~1.65 ppm (–CH_3) and ~2.5 ppm (–CH_3), respectively. Results for EAN–ACN systems are shown in Table 4 and Fig. 5. The value for neat acetonitrile is in excellent agreement with the literature.[48–51] To our knowledge, there are no literature data for the EAN self-diffusion coefficient.

As expected, the value of the self-diffusion coefficients decreases as EAN is added to the system, with the IL being much more viscous than acetonitrile. Considering the mobility of ACN, for $\chi_{EAN} < 0.5$, it is by far more than that of the cation,

Table 3 ^{1}H NMR chemical shifts for EAN–acetonitrile mixtures

χ_{EAN}	$N\equiv CH_3$	H_3C–C(H_2)–NH_3^+	H_3C–C(H_2)–NH_3^+	H_3C–C(H_2)–NH_3^+
0	2.67 ppm	—	—	—
0.1	2.59 ppm	1.85 ppm	3.65 ppm	8.01 ppm
0.3	2.49 ppm	1.73 ppm	3.55 ppm	7.93 ppm
0.5	2.39 ppm	1.60 ppm	3.43 ppm	7.84 ppm
0.7	2.36 ppm	1.57 ppm	3.42 ppm	7.84 ppm
0.9	2.29 ppm	1.53 ppm	3.38 ppm	7.80 ppm
1	—	1.48 ppm	3.34 ppm	7.76 ppm

Table 4 Diffusion coefficients for a cation and acetonitrile obtained by PGSE ^{1}H NMR at 293 K using eqn (6)

	Diffusion coefficient [10^{-11} m^2 s^{-1}]	
χ_{EAN}	Cation	Acetonitrile
0	—	432.57
0.1	79.90	245.00
0.3	28.20	125.00
0.5	18.30	51.00
0.7	16.20	32.00
0.9	15.20	4.52
1	3.80	—

indicating poor correlation between them, while at higher IL concentrations, their transport is much more similar, suggesting interactions between cationic and neutral species. In the inset of Fig. 5, we report the deviation of the diffusivities D from those calculated using the Stoke–Einstein equation

$$D = \frac{k_B T}{c\pi\eta r} \quad (7)$$

where k_B is the Boltzmann constant, r is the effective spherical radius obtained from the van der Waals volume of the molecules,[52,53] and c is a constant that depends on the boundary conditions. A value of 4 is used for slip conditions (low interacting molecules), while 6 is used for stick boundaries (strong interactions between molecules). For our purpose we have used c = 6, thus working in the limit of stick boundary conditions. Large deviations are observed for the measured values relative to the hydrodynamic predictions over the whole concentration range, except for neat EAN and ACN. The cation diffusion is systematically overestimated, while that of acetonitrile is underestimated. Since the cation and ACN are similar in size (r_{EA} = 2.37 Å; r_{ACN} = 2.27 Å), eqn (7) predicts similar D values, while experimentally they exhibit different behaviours. These deviations are linked to the presence of aggregates in the solution, consistent with our other observations.[38] Upon further analysis, representing the PGSE data in a Diffusion Ordered SpectroscopY (DOSY) plot,[54] the dynamics appears to be much

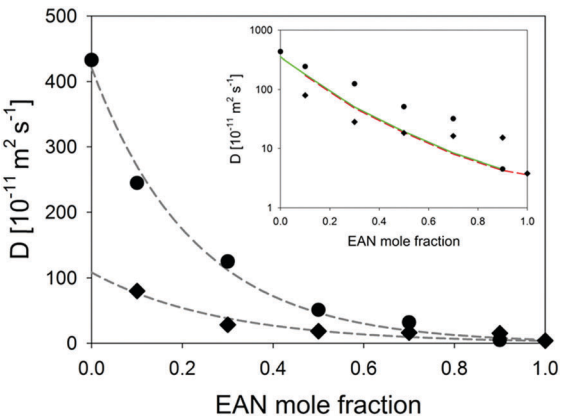

Fig. 5 Diffusion coefficients for ethylammonium nitrate–acetonitrile mixtures. Cation (diamonds); acetonitrile (circles). Dashed line is the fit using an exponential decay function. (inset) Deviation from the Stokes–Einstein equation. Cation (red); acetonitrile (green).

more complicated. Initially, the FID is transformed using the Bayesian transformation[55,56] instead of the Fourier transformation to improve the signal-to-noise ratio. Thereafter, to derive D, a non-linear inversion of the transform is applied to extract the decay constants that are divided by $[-(\gamma\delta)^2(\Delta - \delta/3)]$ and are customarily plotted on a logarithmic scale because diffusion rates typically vary by a few orders of magnitude. Diffusion spectra are then presented as a 2D plot (DOSY plot) with the chemical shift in the horizontal axis and log(D) in the vertical axis.[54] The results are reported in Fig. 6. While the simple fitting procedure implicitly constrains all the molecules of a given species to have a unique D value (single exponential decay), the DOSY approach does not assume any limitation (multiple exponential decays). In the EAN-rich systems (*i.e.* χ_{EAN} = 0.9, 0.7 and partially 0.5) the points corresponding to the cation diffusion are small and well defined, at χ_{EAN} = 0.1 and 0.3 (and partially 0.5) these data are very broad and diffuse.

This leads to a wide distribution of the values of the diffusion coefficient, as is clear from the shape of their distribution that does not appear like a Gaussian-like curve, but rather as a convolution of different curves. This means that there are identical molecules (the cations) in the mixture moving differently because their environment is very different and so experience various interactions. This observation supports our interpretation of structural inhomogeneity given in a recent paper by some of us,[38] where we state that in the EAN-poor region, ILs tend to self-interact, generating strong density fluctuations. Conductivity is another important transport property of ionic liquids,[57–60] since it depends on the mobility of the ions constituting that systems. The conductivity of the EAN–ACN mixtures was measured as a function of temperature and composition. The collected resistivity data for the mixtures at 298 K are shown in Fig. 7. Similar behaviour was observed for the resistivity data at all other measured temperatures *i.e.* 278, 288 and 308 K. The applied frequency ranges from 1 to 100 kHz. This range was chosen because it assures a constant value of the solution resistance. For the sake of comparison a longer scan (to 10 Hz, not shown) was conducted. A reduction in the value of the applied frequency causes a deviation from linearity of the experimental response: higher resistance (*i.e.* lower conductivity) values have been recorded. This observation could be largely expected taking into account the well-known Debye–Falkenhagen effect.[61] Moreover, a low frequency leads to a longer time in which the working electrode experiences the same polarization: the longer time scale leads to a higher probability that some ions could adsorb onto the electrode and thus passivate it. Such passivation leads to higher measured resistance values that are not representative of the real solution resistance.

A similar effect could be due to the formation of a Helmholtz compact layer of ions (anions or cations depending on the electrode positive or negative polarization) that do not allow other carriers to reach the electrode. In order to evaluate the magnitude of those phenomena it is quite important to also know the amplitude of the potential perturbation at the electrode. In this work five different values have been adopted (*i.e.* 10, 20, 50, 100 and 200 mV). From Fig. 7 one can deduce that higher conductivity values could be obtained by increasing the potential perturbation. The enhancement of solution conductivity is due to lowering of both the Wien[62,63] and the

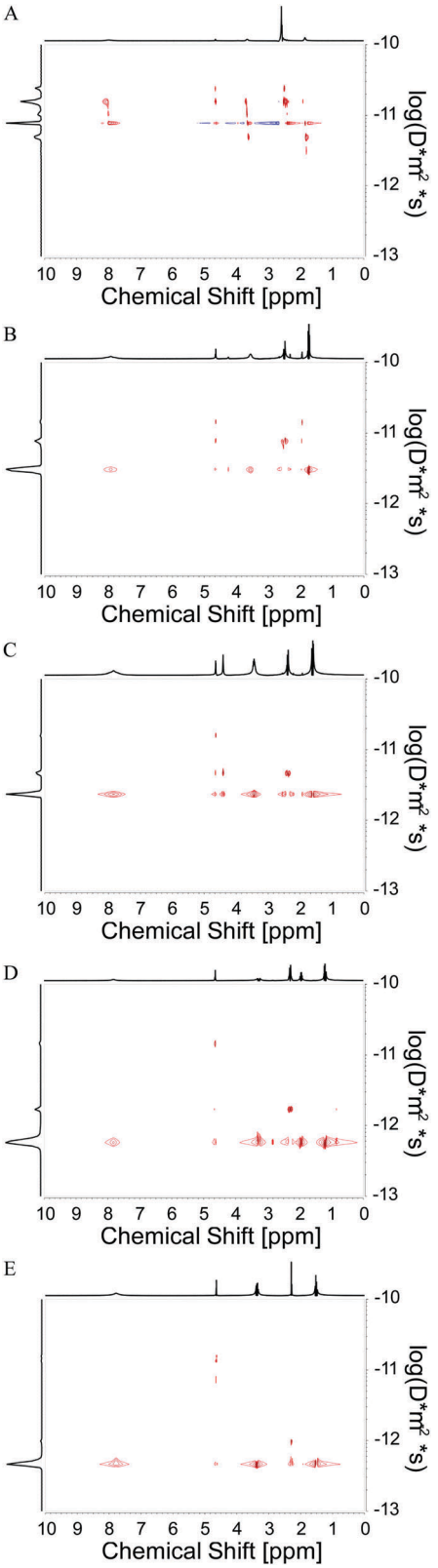

Fig. 6 ^{1}H NMR DOSY spectra for ethylammonium nitrate–acetonitrile mixtures. (A) χ_{EAN} = 0.1; (B) 0.3; (C) 0.5; (D) 0.7; (E) 0.9.

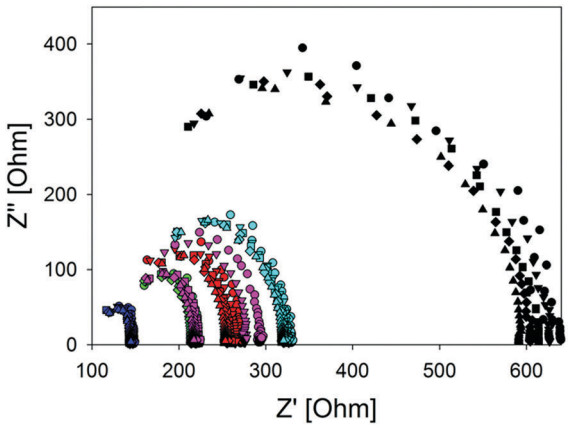

Fig. 7 Impedance curves obtained from the EIS analysis of the ethylammonium nitrate–acetonitrile mixtures at 298 K. χ_{EAN} = 0.1 (black); 0.2 (red); 0.3 (green); 0.5 (blue); 0.7 (purple); 0.9 (cyan). Different symbols refer to different potential perturbations. 10 mV (circles); 20 mV (reversed triangles); 50 mV (squares); 100 mV (diamonds); 200 mV (triangles).

Falkenhagen effects. Despite the small difference, the value obtained with the application of the higher perturbation (200 mV) will be presented throughout the work. The trend of the conductivity with the composition is more complicated to analyse. The resistance of the mixtures increases in the order (χ_{EAN}) 0.5–0.3 < 0.2–0.7 < 0.9 < 1 < 0.1 < 0. The conductivity κ is proportional to the number of charge carriers n and to the ionic mobility μ[64]

$$\kappa = \sum nZe\mu \quad (8)$$

where Z is the ion charge, and e is the charge of the electron. By increasing the EAN mole fraction, the number of charge carriers grows but the solution exhibits a higher viscosity. The maximum value of conductivity (*i.e.* $0.3 \leq \chi_{EAN} \leq 0.5$) is reached when n assures a good charge transport and η is not so high to reduce the latter's mobility. Either reducing the concentration of charge carriers or increasing the viscosity will lead to a reduction in the conductivity of the mixture. Interestingly, the depletion of conductivity upon increasing the concentration of the IL from χ_{EAN} = 0.7 to 0.9 is quite small. Theoretically, some ion pairs could be generated because of the increase of IL mole fraction, which becomes the dominant species in the mixture. The relative high conductivity value (31.4 mS cm^{-1}) recorded for the χ_{EAN} = 0.9 mixture allows us to conclude that only a limited number of ion pairs could be generated. Every system under investigation experiences an increase of conductivity with the increase of polarization as expected for ionic conductors that undergo the Wien effect.[62,63] We want to highlight the particular case of the χ_{EAN} = 0.7 mixture, where such an increase is anomalously high. This mixture shows an expected value of conductivity when the applied potential is higher (*i.e.* 200, 100 and 50 mV). When the magnitude of this potential is decreased (*i.e.* to 20 and 10 mV) the mixture becomes unexpectedly more resistive (~300 Ω). This observation is independent of the experimental temperature. The choice of 200 mV as a perturbation potential removes this unusual behaviour. Nevertheless, this observation will be explored in more detail in a forthcoming paper. From the experimental resistivity ρ, we computed the molar conductivities from

$$\kappa = \frac{1}{\rho} \quad (9)$$

$$\Lambda_m = \frac{\kappa}{[EAN]} \quad (10)$$

where Λ_m is the molar conductivity, and [EAN] is the IL molarity. Results are plotted in Fig. 8. The measured conductivity data are reported in the ESI,† Table S3. The absence of the values for pure EAN conductivities at lower temperatures (*i.e.* 278 and 288 K) results from the relatively high melting point of 289 K. These data were interpolated using a modified Onsager equation[65,66]

$$\Lambda_m = a_1 - a_2\sqrt{\chi_{EAN}} + a_3\chi_{EAN}\ln(\chi_{EAN}) + a_4\chi_{EAN} + a_5{\chi_{EAN}}^2 \quad (11)$$

where a_n are numerical coefficients. The values of conductivity that we determined at ambient temperature are sensibly higher if they are compared to others previously reported in the literature (see Table S4 in ESI†). This inconsistency is trivially explained by taking into account the different fitting procedures adopted to extrapolate the values. Sonnleitner *et al.* extrapolated R_{inf} values from measurements ranging from 10 kHz to 480 Hz. In our experiments such an approach could not be considered valid. This is because of the loss of linearity in resistance occurring at frequencies lower than 1 kHz. Therefore, we have fitted experimental values which were recorded in the frequency range 1–100 kHz. Under these conditions, the ionic conductivity of the samples can be estimated more accurately. Nevertheless, for the sake of comparison, we also report values obtained using the fitting procedure proposed by Sonnleitner *et al.* The obtained values are in very good agreement with the ones reported previously, since only two samples show differences larger than 5%. The molar conductivity displays a maximum for $\chi_{EAN} \sim 0.2$. The latter evidence is in very good agreement with the computational analyses (see ref. 38) where, in this composition

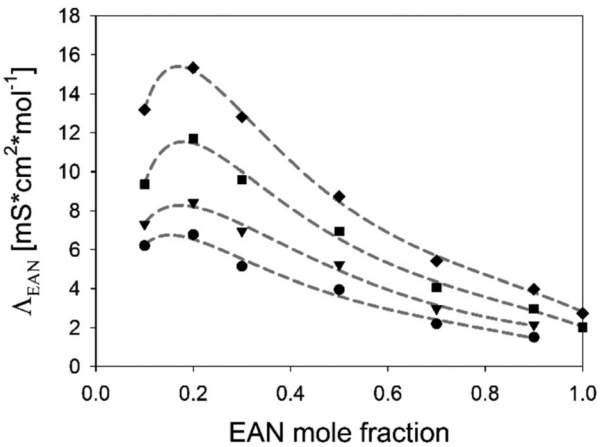

Fig. 8 Molar conductivity for ethylammonium nitrate–acetonitrile mixtures at different temperatures. 278 K (circles); 288 K (triangles); 298 K (squares); 308 K (diamonds).

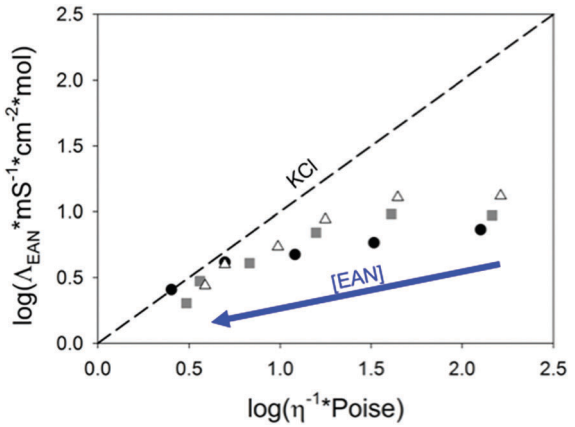

Fig. 9 Walden plot for ethylammonium nitrate–acetonitrile mixtures at different temperatures and compositions. 288 K (circles); 298 K (squares); 308 K (triangles). EAN content increases according to the direction of the arrow from χ_{EAN} = 0.1 to 1 in increments of 0.1. The dashed line represents the "ideal" KCl 0.01 M trend.

region, the IL arranges in a quite unexpected channel-like structure. The conductivity maximum is slightly dependent on the temperature, as it is shifted towards more dilute compositions cooling the system. This is probably because we are near the melting point of EAN, so the more the IL in the mixture, the lower conductivity because of EAN incipient solidification. Interestingly, this trend in conductivity is quite different from those observed for viscosity and diffusivity: the former monotonically decreases as ACN is added to EAN while the latter increases. Such differences in behaviour are probably due to strong ion pairing effects. Pure ACN exhibits zero conductivity. Upon addition of EAN the molar conductivity increases. As previously stated, the molar conductivity reaches its maximum at a 4 : 1 ACN/EAN ratio. By moving this ratio towards an EAN richer composition, the values decrease exponentially. In fact, despite its relatively high dielectric constant (38.8), ACN is not able to efficiently solvate the EAN cations and anions, leading to the formation of ion pairs. Thus, future work can address ion pairing effects by considering the anionic diffusivities to complement the ACN and cationic diffusivities reported here. The steric hindrance of ion pairs is obviously higher than the separate ions and their localized charge is clearly lower: the change of these two factors leads to lowering of the ionic mobility and molar conductivity.

It is clear that by increasing the EAN mole fraction, the formation of ion pairs is facilitated. Obviously, conductivity also depends on the viscosity of the media. A Walden plot directly relates these two quantities,[67] as shown in Fig. 9. An increasing deviation from the ideal 0.01 M KCl line is observed as acetonitrile is added to the ionic liquid, and this trend is always the same regardless of the temperature. Following the qualitative interpretation given by Angell *et al.*,[68] systems that lie below the ideal line are characterized by progressively more ionic pairing, proportionally to the distance from the ideal 0.01 M KCl line that represent a fully dissociated system. This observation, together with the deviation from the Stokes–Einstein equation, suggests that ethylammonium nitrate is progressively induced to self-associate as the ACN content of the mixture is increased. The observation that EAN acts as a dissociated electrolyte in the neat state and progressively binds itself when acetonitrile is added to the system is a quite strong confirmation that ILs (including protic ionic liquids) are concentrated electrolytes rather than dilute ones, in line with the statements from Sha *et al.*[69] and Lee *et al.*[70] Indeed we do not observe any dynamic, structural[38] or computational[38] evidence of extended ionic pairing in pure or concentrated IL systems, whereas in the dilute regime the ions associate leading to a divergence from the KCl line in the Walden plot. This behaviour is in accord with our recent structural observations (see ref. 38), thus confirming the overall inhomogeneity of IL-poor EAN–acetonitrile mixtures.

Conclusions

In summary, we have studied the transport properties of binary mixtures of ethylammonium nitrate and acetonitrile. Our findings suggest that a complex series of interactions govern the dynamics of the mixtures both at micro and macroscopic scales. Shear viscosity is one metric for the overall molecular mobility and shows strong deviations for this system. Such behaviour may be ascribed to the formation of large scale aggregates that behave similarly to colloidal aggregates, increasing the viscosity in the EAN-rich region. At the molecular-size level, the diffusion coefficients of acetonitrile and the cation show a marked inhomogeneity in the EAN-poor regime, suggesting that the samples are far to be ideally mixed, and identical molecules experience different environments within the same system. Looking directly to the mobility of the ionic liquid itself, the conductivity measures also suggest strong ionic pairing in the EAN-poor region, but the specific structure that is adopted by the IL at those compositions, together with the lowered viscosity, is responsible for an enhanced conductive power of these mixtures. In conclusion, we have observed that the EAN–acetonitrile mixtures exhibit a marked mesoscopic inhomogeneity that strongly affects the transport properties of the system.

Experimental section

Ethylammonium nitrate was purchased from IoLiTec ($>98\%_{wt}$) and was pumped under high vacuum by slightly heating at 50 °C overnight to remove residual water. The final content of water was checked using ^{1}H NMR and it was undetectable ($<0.02\%_{wt}$). Anhydrous acetonitrile was purchased from Sigma Aldrich ($99.8\%_{wt}$) and used without further treatment. This sets uncertainty in the mixture composition below $1.5\%_{mol}$. All the samples were prepared by weighing in a controlled atmosphere of dry argon. Viscosities of the EAN–ACN mixtures were measured using a temperature-controlled ViscoLab 4100 automated viscometer from Cambridge Viscosity. The temperature was controlled by flowing water from a Lauda Brinkmann RMT-6 recirculating chiller through a temperature-controlled stainless steel jacket surrounding the viscometer, which had an internal thermocouple. Temperatures

were controlled to ±0.1 K. Each EAN–ACN mixture was equilibrated for at least 15 minutes before viscosity measurements. Magnetic stainless pistons of varying diameters were used depending on the viscosity range. The viscometer was placed inside a plastic glove bag that was continuously purged with nitrogen. Viscosities of the mixtures were well fitted by the Arrhenius law. Pulsed-Gradient Spin-Echo NMR experiments[45–47] were used to measure self-diffusion coefficients of ethylammonium cations and acetonitrile solvent molecules in the EAN–ACN mixtures. A Varian DirectDrive instrument operating at ^{1}H frequencies of 400 MHz was used, consistent with our prior measurement techniques.[6,7,71] The Varian implementation of the bipolar pulse pair stimulated echo pulse sequence[47] was used (*dbppste*). The gradient probe used was a Doty Scientific model 16-38. Field strengths ranging from 5 to 200 G cm^{-1} were used. Conductivity measurements were carried out using a conductivity electrode (5072 from Crison, K = 10 cm^{-1}) with a platinum plate for both working and counter electrodes. The electrode was coupled to an Autolab potentiostat/galvanostat Model PGSTAT12® from Metrohm. The potentiostat/galvanostat was remotely controlled by the computer using Nova 1.9 software. An electrochemical impedance scan was employed to measure the A.C. resistance of each solution, from which the relative conductivity was calculated. In the EIS experiments the amplitude of the potential perturbation ranged from 10 to 200 mV. Impedance spectra were recorded within the frequency ranges 10^3–10^6 Hz. During each measurement, temperature was kept constant at each desired value using a water-bath thermostat. The temperature uncertainty is below 0.5 K. The overall error in each reported value is below 5%.

Conflicts of interest

There are no conflicts to declare.

Acknowledgements

We would like to acknowledge Prof. Ruggero Caminiti for the valuable effort and the insightful discussions. A. Mariani acknowledges the PhD commission of La Sapienza University of Rome for having funded the mission in USA. B. Wu and E. Castner were supported by the U.S. National Science Foundation grant CHE-1362272. D. Dini and M. Bonomo acknowledge the financial support from the University of Rome "La Sapienza" through the program Ateneo 2016.

Notes and references

1 R. D. Rogers, *Science*, 2003, **302**, 792–793.
2 M. Armand, F. Endres, D. R. MacFarlane, H. Ohno and B. Scrosati, *Nat. Mater.*, 2009, **8**, 621–629.
3 E. W. Castner, Jr. and J. F. Wishart, *J. Chem. Phys.*, 2010, **132**, 120901.
4 T. L. Greaves and C. J. Drummond, *Chem. Rev.*, 2015, **115**, 11379–11448.
5 X. Wang, Y. Chi and T. Mu, *J. Mol. Liq.*, 2014, **193**, 262–266.
6 M. Liang, S. Khatun and E. W. Castner, Jr., *J. Chem. Phys.*, 2015, **142**, 121101.
7 T. A. Fadeeva, P. Husson, J. A. DeVine, M. F. Costa Gomes, S. G. Greenbaum and E. W. Castner, Jr., *J. Chem. Phys.*, 2015, **143**, 64503.
8 K. R. Seddon, A. Stark and M.-J. Torres, *Pure Appl. Chem.*, 2000, **72**, 2275–2287.
9 U. Domańska and M. Laskowska, *J. Chem. Eng. Data*, 2009, **54**, 2113–2119.
10 U. Domańska and M. Laskowska, *J. Solution Chem.*, 2009, **38**, 779–799.
11 P. Walden, *Bull. Acad. Imp. Sci. St.-Petersbourg*, 1914, **8**, 405–422.
12 A. Oleinikova and M. Bonetti, *J. Solution Chem.*, 2002, **31**, 397–413.
13 R. Atkin and G. G. Warr, *J. Phys. Chem. B*, 2008, **112**, 4164–4166.
14 R. Hayes, S. Imberti, G. G. Warr and R. Atkin, *Angew. Chem., Int. Ed.*, 2012, **51**, 7468–7471.
15 K. Fumino, A. Wulf and R. Ludwig, *Angew. Chem., Int. Ed.*, 2009, **48**, 3184–3186.
16 O. Russina, M. Macchiagodena, B. Kirchner, A. Mariani, B. Aoun, M. Russina, R. Caminiti and A. Triolo, *J. Non-Cryst. Solids*, 2015, **407**, 333–338.
17 A. Mariani, O. Russina, R. Caminiti and A. Triolo, *J. Mol. Liq.*, 2015, **212**, 947–956.
18 R. Zarrougui, M. Dhahbi and D. Lemordant, *J. Solution Chem.*, 2010, **39**, 1531–1548.
19 V. N. Emel'yanenko, G. Boeck, S. P. Verevkin and R. Ludwig, *Chem. – Eur. J.*, 2014, **20**, 11640–11645.
20 H. Weingärtner, A. Knocks, W. Schrader and U. Kaatze, *J. Phys. Chem. A*, 2001, **105**, 8646–8650.
21 R. Zarrougui, M. Dhahbi and D. Lemordant, *J. Solution Chem.*, 2015, **44**, 686–702.
22 J. A. Smith, G. B. Webber, G. G. Warr and R. Atkin, *J. Phys. Chem. B*, 2013, **117**, 13930–13935.
23 T. L. Greaves, D. F. Kennedy, N. Kirby and C. J. Drummond, *Phys. Chem. Chem. Phys.*, 2011, **13**, 13501.
24 B. Docampo-Álvarez, V. Gómez-González, T. Méndez-Morales, J. Carrete, J. R. Rodríguez, Ó. Cabeza, L. J. Gallego and L. M. Varela, *J. Chem. Phys.*, 2014, **140**, 214502.
25 A. Mariani, R. Dattani, R. Caminiti and L. Gontrani, *J. Phys. Chem. B*, 2016, **120**, 10540–10546.
26 G. Perron, A. Hardy, J.-C. Justice and J. E. Desnoyers, *J. Solution Chem.*, 1993, **22**, 1159–1178.
27 P. M. Mancini, G. G. Fortunato and L. R. Vottero, *Phys. Chem. Liq.*, 2004, **42**, 625–632.
28 T. Sonnleitner, V. Nikitina, A. Nazet and R. Buchner, *Phys. Chem. Chem. Phys.*, 2013, **15**, 18445.
29 S. Song and C. Peng, *J. Dispersion Sci. Technol.*, 2008, **29**, 1367–1372.
30 T. Ono, R. Amezawa, A. Igarashi, M. Ota, Y. Sato and H. Inomata, *Fluid Phase Equilib.*, 2016, **407**, 198–208.
31 P. S. Nikam, B. S. Jagdale, A. B. Sawant and M. Hasan, *J. Chem. Eng. Data*, 2000, **45**, 559–563.
32 A. Chagnes, A. Tougui, B. Carré, N. Ranganathan and D. Lemordant, *J. Solution Chem.*, 2004, **33**, 247–255.

33 A. R. Mahajan and S. R. Mirgane, *J. Thermodyn.*, 2013, **2013**, 1–11.
34 O. Redlich and A. T. Kister, *Ind. Eng. Chem.*, 1948, **40**, 345–348.
35 J. E. Desnoyers and G. Perron, *J. Solution Chem.*, 1997, **26**, 749–755.
36 Z. P. McAtee and M. P. Heitz, *J. Chem. Thermodyn.*, 2016, **93**, 34–44.
37 M. P. Heitz, *J. Chem. Thermodyn.*, 2017, **108**, 143–144.
38 A. Mariani, R. Caminiti, F. Ramondo, G. Salvitti, F. Mocci and L. Gontrani, *J. Phys. Chem. Lett.*, 2017, **8**, 3512–3522.
39 S. B. Capelo, T. Méndez-Morales, J. Carrete, E. López Lago, J. Vila, O. Cabeza, J. R. Rodríguez, M. Turmine and L. M. Varela, *J. Phys. Chem. B*, 2012, **116**, 11302–11312.
40 M. Geppert-Rybczyńska, J. K. Lehmann and A. Heintz, *J. Chem. Thermodyn.*, 2014, **71**, 171–181.
41 P. Navia, J. Troncoso and L. Romaní, *J. Solution Chem.*, 2008, **37**, 677–688.
42 B. Mokhtarani, A. Sharifi, H. R. Mortaheb, M. Mirzaei, M. Mafi and F. Sadeghian, *J. Chem. Thermodyn.*, 2009, **41**, 1432–1438.
43 A. Drozd-Rzoska and S. J. Rzoska, *NATO Science for Peace and Security Series A: Chemistry and Biology*, Springer, Dordrecht, 2010, pp. 93–106.
44 A. Mariani, R. Caminiti, M. Campetella and L. Gontrani, *Phys. Chem. Chem. Phys.*, 2016, **18**, 2297–2302.
45 E. O. Stejskal, *J. Chem. Phys.*, 1965, **43**, 3597–3603.
46 J. E. Tanner, *J. Chem. Phys.*, 1970, **52**, 2523–2526.
47 D. H. Wu, A. D. Chen and C. S. Johnson, *J. Magn. Reson., Ser. A*, 1995, **115**, 260–264.
48 A. Easteal, *Aust. J. Chem.*, 1980, **33**, 1667.
49 H. G. Hertz and H. Leiter, *Z. Phys. Chem.*, 1982, **133**, 45–67.
50 E. Hawlicka, *Z. Naturforsch., A: Phys. Sci.*, 1988, **43**, 769–773.
51 T. Takamuku, M. Tabata, A. Yamaguchi, J. Nishimoto, M. Kumamoto, H. Wakita and T. Yamaguchi, *J. Phys. Chem. B*, 1998, **102**, 8880–8888.
52 J. T. Edward, *J. Chem. Educ.*, 1970, **47**, 261.
53 H. Zhao, *Phys. Chem. Liq.*, 2003, **41**, 545–557.
54 B. Antalek, *Concepts Magn. Reson.*, 2002, **14**, 225–258.
55 G. L. Bretthorst, *J. Magn. Reson.*, 1990, **88**, 533–551.
56 D. Xing, S. J. Gibbs, J. A. Derbyshire, E. J. Fordham, T. A. Carpenter and L. D. Hall, *J. Magn. Reson., Ser. B*, 1995, **106**, 1–9.
57 V. V. Chaban, I. V. Voroshylova, O. N. Kalugin and O. V. Prezhdo, *J. Phys. Chem. B*, 2012, **116**, 7719–7727.
58 A. Jarosik, S. R. Krajewski, A. Lewandowski and P. Radzimski, *J. Mol. Liq.*, 2006, **123**, 43–50.
59 J. N. Canongia Lopes, M. F. Costa Gomes, P. Husson, A. A. H. Pádua, L. P. N. Rebelo, S. Sarraute and M. Tariq, *J. Phys. Chem. B*, 2011, **115**, 6088–6099.
60 C. Zhao, G. Burrell, A. A. J. Torriero, F. Separovic, N. F. Dunlop, D. R. MacFarlane and A. M. Bond, *J. Phys. Chem. B*, 2008, **112**, 6923–6936.
61 J. Anderson, *J. Non-Cryst. Solids*, 1994, **172–174**, 1190–1194.
62 M. Wien, *Ann. Phys.*, 1927, **83**, 305.
63 M. Wien, *Ann. Phys.*, 1928, **85**, 795.
64 I. N. Levine, *Physical Chemistry*, McGraw-Hill, Boston, MA, 5th edn, 2002.
65 L. Onsager and R. M. Fuoss, *J. Phys. Chem.*, 1931, **36**, 2689–2778.
66 A. Stoppa, J. Hunger and R. Buchner, *J. Chem. Eng. Data*, 2009, **54**, 472–479.
67 C. Schreiner, S. Zugmann, R. Hartl and H. J. Gores, *J. Chem. Eng. Data*, 2010, **55**, 1784–1788.
68 C. A. Angell, N. Byrne and J.-P. Belieres, *Acc. Chem. Res.*, 2007, **40**, 1228–1236.
69 M. Sha, H. Dong, F. Luo, Z. Tang, G. Zhu and G. Wu, *J. Phys. Chem. Lett.*, 2015, **6**, 3713–3720.
70 A. A. Lee, D. Vella, S. Perkin and A. Goriely, *J. Phys. Chem. Lett.*, 2015, **6**, 159–163.
71 S. H. Chung, R. Lopato, S. G. Greenbaum, H. Shirota, E. W. Castner, Jr. and J. F. Wishart, *J. Phys. Chem. B*, 2007, **111**, 4885–4893.

